Photothermic regulation of gene expression triggered by laser-induced carbon nanohorns

Eijiro Miyako[a,1], Tomonori Deguchi[b], Yoshihiro Nakajima[c], Masako Yudasaka[d], Yoshihisa Hagihara[a], Masanori Horie[a,2], Mototada Shichiri[a], Yuriko Higuchi[e], Fumiyoshi Yamashita[e], Mitsuru Hashida[e], Yasushi Shigeri[a], Yasukazu Yoshida[a,c], and Sumio Iijima[d,f,g,1]

[a]Health Research Institute, National Institute of Advanced Industrial Science and Technology, Osaka 563-8577, Japan; [b]Health Research Institute, National Institute of Advanced Industrial Science and Technology, Hyogo 661-0974, Japan; [c]Health Research Institute, National Institute of Advanced Industrial Science and Technology, Kagawa 761-0395, Japan; [d]Nanotube Research Center, National Institute of Advanced Industrial Science and Technology, Ibaraki 305-8565, Japan; [e]Department of Drug Delivery Research, Graduate School of Pharmaceutical Sciences, Kyoto University, Kyoto 606-8501, Japan; [f]Meijo University, Nagoya 468-8502, Japan; and [g]NEC, Ibaraki 305-8501, Japan

Contributed by Sumio Iijima, April 3, 2012 (sent for review February 2, 2012)

The development of optical methods to control cellular functions is important for various biological applications. In particular, heat shock promoter-mediated gene expression systems by laser light are attractive targets for controlling cellular functions. However, previous approaches have considerable technical limitations related to their use of UV, short-wavelength visible (vis), and infrared (IR) laser light, which have poor penetration into biological tissue. Biological tissue is relatively transparent to light inside the diagnostic window at wavelengths of 650–1,100 nm. Here we present a unique optical biotechnological method using carbon nanohorn (CNH) that transforms energy from diagnostic window laser light to heat to control the expression of various genes. We report that with this method, laser irradiation within the diagnostic window resulted in effective heat generation and thus caused heat shock promoter-mediated gene expression. This study provides an important step forward in the development of light-manipulated gene expression technologies.

carbon nanotube | cell | phototherapy

The development of noninvasive remote control technologies to manipulate cellular functions (1–13) is important for various biological applications, including cancer research, immunology, tissue engineering, and brain science. In particular, optical regulation of gene expression (1–8) and optogenetic control of receptor and channel proteins on the cell surface (9–13) have received much research attention. Heat shock proteins (HSPs) are critical components of a cell's defense mechanism against injury associated with adverse stresses (14–18). Promoters that contain heat shock elements (HSEs) upstream of the HSP coding region, known as heat shock promoters, can be turned on by various stresses besides heat shock, including heavy ions, radicals, alcohol, and viral infection, suggesting that they are driven by almost all kinds of stresses (1–8, 14–18). Given the simple and highly controllable nature of heat shock treatment, the heat shock response is ubiquitous in all organisms from bacteria to higher vertebrates. Numerous researchers have pursued regulated gene expression by heat shock in mammals, fish, and other organisms (1–8). Thus, heat shock response-affected gene expression systems are attractive targets for controlling cellular functions.

Light-driven gene expression techniques have been developed using UV (1–3), short-wavelength visible (vis) (4, 5), and IR (6–8) laser light heat to induce a heat shock response, which acts as a trigger to drive expression of genes inserted downstream of heat shock promoters. UV, short-wavelength vis, and IR light have poor penetration into biological tissue, whereas near-infrared (NIR) laser light (wavelength 0.7–2.5 μm) can penetrate at least 10 cm through deep tissue (19, 20). Biological systems are transparent to light within the diagnostic window, that is, within 650–1,100 nm (19). Nanocarbons, such as carbon nanotubes (CNTs) and carbon nanohorn (CNH), are considered useful in science and technology because of their remarkable physical and chemical properties, some of which might help overcome the limitations of traditional laser light technologies. In particular, nanocarbons have extraordinary photothermal energy conversion efficiency and high absorption cross-sections in a wavelength range capable of transmission within the diagnostic window (21–38). Although gold nanoparticles also have such photothermal properties, nanocarbons can be more effectively heated at various wavelengths because of their strong absorbance over a wide range of the optical region (38). Potential problems exist with CNT biocompatibility, however, including impurities in the metal catalysts used in CNT synthesis (39, 40). Conversely, CNHs are produced without metal catalysts and have relatively low toxicity, as shown in both in vitro and in vivo experiments (41–45). Thus, CNHs appear to be more amenable than CNTs for use in various biomedical and biotechnological applications. Here we show that CNH complexes with BSA (BSA–CNH) are well dispersed in aqueous solutions and can effectively convert light energy to thermal energy. These complexes introduced into various cells and transgenic medaka (*Oryzias latipes*) can supply the thermal energy necessary for heat shock promoter-mediated gene expression. Low-power laser irradiation of CNH remotely controls the supply of this energy, and this energy effectively drives gene expression in living mice. Thus, nanocarbons dramatically extend the concept of optical regulation of cellular functions.

Results and Discussion

Characterization of BSA–CNH. To construct the regulatory system of heat shock promoter-mediated gene expression inducible by the photothermal properties of nanocarbons, we first prepared water-dispersible CNH complexes (Fig. 1). Given the hydrophobic nature of CNHs (26–28), we complexed them with commercially available low-bioactive BSA molecules through low-power (80 W) facile ultrasonic treatment (Fig. 1*A*). The resulting BSA–CNH complexes were well dispersed in several aqueous solutions (Fig. 1*B*, *Inset*). The UV–vis–NIR optical absorption spectrum of PBS dispersions of BSA–CNH peaked at 260 nm (Fig. 1*B*), characteristic of the absorption of tubular graphite and BSA molecules (27, 28, 44). The BSA–CNH complexes were ~100–200 nm in diameter as estimated by atomic force microscopy and dynamic light scattering

Author contributions: E.M. and S.I. designed research; E.M., T.D., Y.N., M. Horie, M.S., and Y. Higuchi performed research; Y. Higuchi, F.Y., and M. Hashida contributed new reagents/analytic tools; E.M., M.Y., Y. Hagihara, Y.S., Y.Y., and S.I. analyzed data; and E.M. and S.I. wrote the paper.

The authors declare no conflict of interest.

Freely available online through the PNAS open access option.

[1]To whom correspondence may be addressed. E-mail: e-miyako@aist.go.jp or iijimas@meijo-u.ac.jp.

[2]Present address: Department of Occupational Pneumology, Institute of Industrial Ecological Sciences, University of Occupational and Environmental Health, Fukuoka 807-8555, Japan.

This article contains supporting information online at www.pnas.org/lookup/suppl/doi:10.1073/pnas.1204391109/-/DCSupplemental.

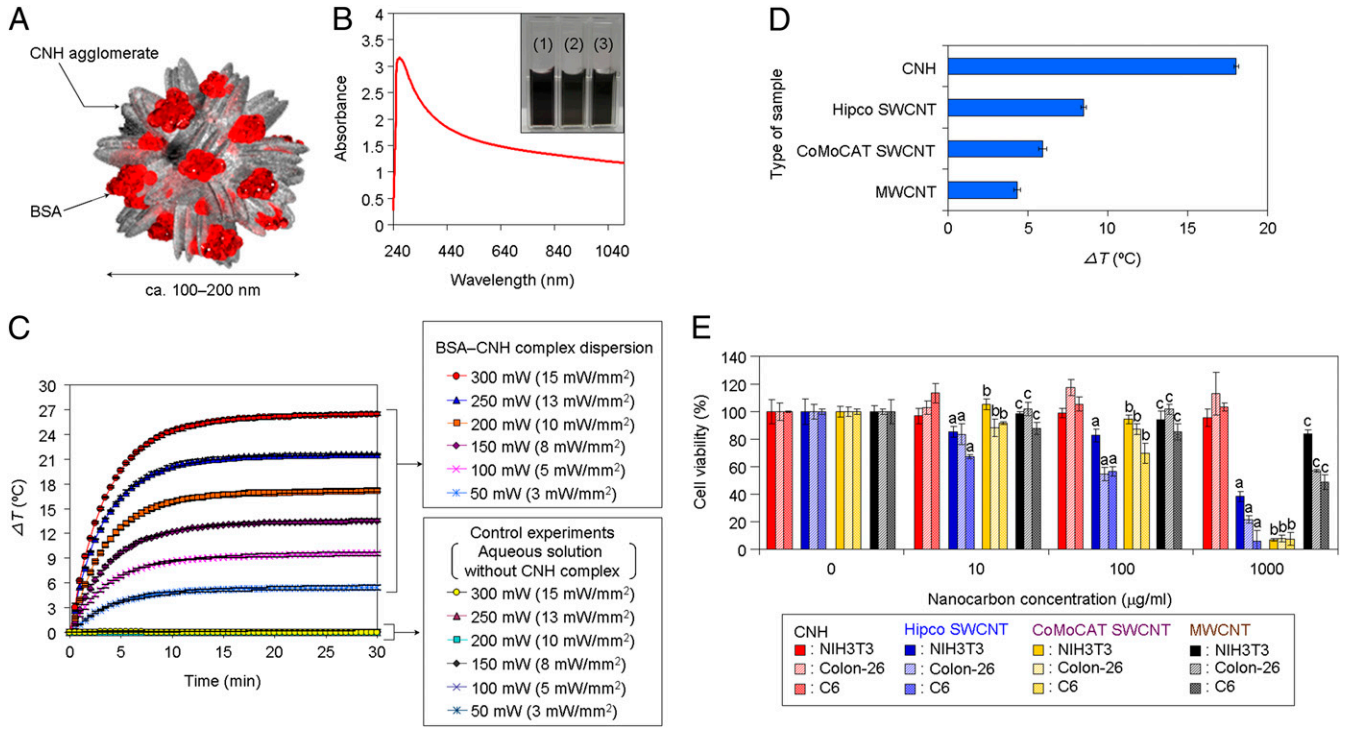

Fig. 1. Characterization of BSA–CNH complexes. (*A*) Schematic illustration of the BSA–CNH complex. (*B*) UV–vis–NIR spectrum of BSA–CNH in PBS buffer. (*Inset*) Photograph of BSA–CNH complex dispersions in (1) DMEM, (2) PBS, and (3) artificial seawater. (*C*) Temperature changes in BSA–CNH complex dispersions under continuous 670-nm laser irradiation at various power levels: 50 mW (~3 mW/mm^2), 100 mW (~5 mW/mm^2), 150 mW (~8 mW/mm^2), 200 mW (~10 mW/mm^2), 250 mW (~13 mW/mm^2), and 300 mW (~15 mW/mm^2). (*D*) Temperature changes in various nanocarbon complexes under continuous 785-nm laser irradiation at 300 mW (~24 mW/mm^2) for 5 min. Hipco, high-pressure carbon monoxide; CoMoCAT, cobalt–molybdenum catalyst. (*E*) Cytotoxicity tests of various BSA–functionalized nanocarbon complexes in NIH 3T3, Colon-26, and C6 cells. The standardized percentage of mitochondrial enzyme activity compared with control. Statistical analyses were performed using ANOVA (Tukey's test). $^{a}P < 0.0005$; $^{b}P < 0.0001$; $^{c}P < 0.025$.

analyses (*SI Appendix*, Fig. S1 *A* and *B*). An aqueous CNH complex dispersion (CNH concentration, 100 μg/mL) exhibited a significant increase in temperature over time (26–28) under 670-nm laser irradiation and with an increase in laser power, whereas control dispersions without CNH complexes showed no increase in temperature at all laser powers (Fig. 1*C*). Moreover, there was no sedimentation of the functionalized CNH complexes, even at a relatively high laser power of 300 mW (laser power density, ~15 mW/mm^2) (*SI Appendix*, Fig. S1*C*). Temperature differences (ΔT) of BSA–CNH complexes were higher than those of other BSA-functionalized CNT (BSA–CNT) complexes with single-walled CNTs or multiwalled CNTs under 785-nm laser irradiation, likely because of the greater water dispersibility of BSA–CNH (Fig. 1*D* and *SI Appendix*, Fig. S2). In the present study, we used two laser wavelengths, because CNH complexes have high optical absorbance over a wide range of wavelengths (Fig. 1*B*).

We next investigated the influence of various BSA-functionalized nanocarbon complexes on mitochondrial enzyme activity in cells, using a 2-(4-iodophenyl)-3-(4-nitrophenyl)-5-(2,4-disulfophenyl)-2H-tetrazolium monosodium salt (WST-1) assay (*SI Appendix*, Fig. S1 *D–F*). BSA–CNH demonstrated low cytotoxicity in various cultured cells, including mouse fibroblasts (NIH 3T3), mouse colon cancer (Colon-26), and rat C6 glioma (C6) cells, although it was absorbed by cells by endocytosis (*SI Appendix*, Fig. S3) (44, 45). The low CNH toxicity was also confirmed in both in vitro (41, 44, 45) and in vivo studies (41–43). We found that BSA–CNH has lower cytotoxicity than BSA–CNTs (Fig. 1*E*). BSA-modified single-walled CNTs have relatively high toxicity compared with other nanocarbons because of metal impurities and/or long, rigid morphology (39, 40). The deleterious effects of multiwalled CNTs on cells are associated with the CNTs' diameter and length (46, 47). Despite these studies, the detailed mechanisms of toxicity of nanocarbons remain unclear. In any case, these results clearly demonstrate that BSA–CNH has many properties important for the control of cellular functions, including powerful photothermal performance, high photostability, low cytotoxicity, and high water dispersibility.

Gene Expression Triggered by Laser-Induced CNH Complexes. The aim of this study was to remotely control heat shock promoter-mediated gene expression using heat converted by BSA–CNH from laser light with a wavelength within the diagnostic window. In our first system, we analyzed laser-triggered remote gene expression in various cells and transgenic medaka (Fig. 2). The ultimate goal of our research is to detect the expression of various exogenous genes inserted downstream of heat shock promoters. In the present study, we selected GFP, red fluorescent protein (DsRed), and luciferase as model targeted genes for expression via heat shock promoter. These proteins are beneficial in that they are directly visualized by the fluorescent microscopy and bioimaging analyzers. In contrast, we chose the HSP70 promoter as a model promoter for gene expression, because its functions are relatively well understood in various HSP family members (14–18). In addition, many previous researchers have examined regulation of gene expression by the HSP70 promoter (1–8).

We measured fluorescent protein expression in three stably transfected cell lines to determine whether the heat shock process was triggered by heat transferred from laser light by BSA–CNH present in the cell culture medium (Fig. 2*A*). We chose NIH 3T3, Colon-26, and C6 cells as gene expression models based on their ease of transfection and handling. GFP from *Aequorea victoria* (48) and DsRed from *Anthozoa* species were the two reporter

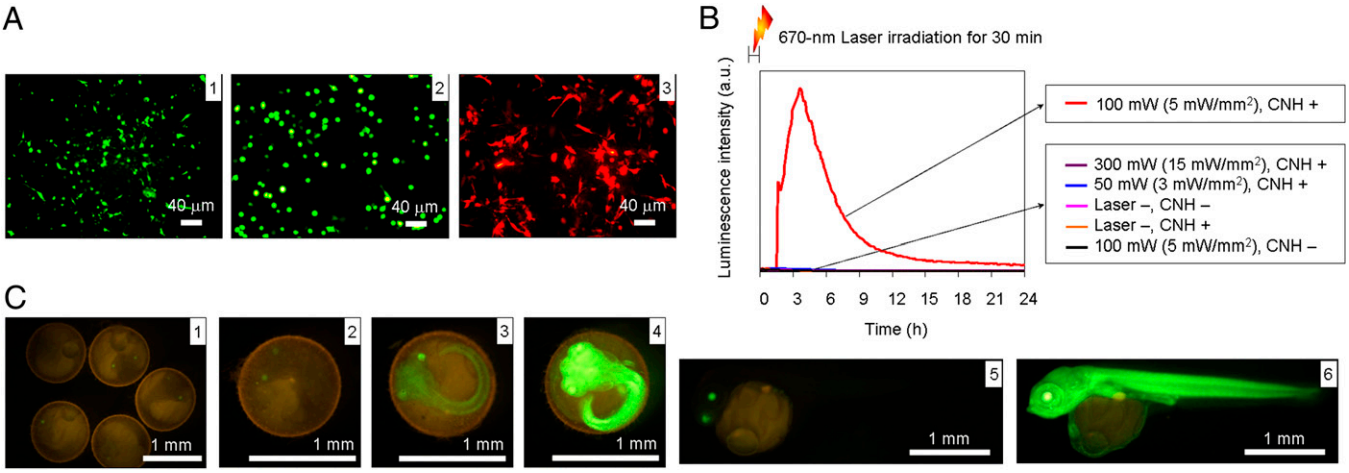

Fig. 2. Photothermic regulation of gene expression in cells and transgenic medaka. (*A*) Expression of fluorescent proteins in (1) NIH 3T3, (2) Colon-26, and (3) C6 cells driven by laser-induced CNH complexes. Cells were irradiated at various laser powers, and expression of fluorescent proteins was observed by fluorescence microscopy. Laser power: (1) 150 mW (~12 mW/mm^2; laser wavelength, 670 nm; (2) 210 mW (~11 mW/mm^2; laser wavelength, 785 nm); (3) 140 mW (~7 mW/mm^2; laser wavelength, 785 nm). (*B*) Real-time monitoring of luciferase expression in NIH 3T3 cells after 670-nm laser irradiation for 30 min at various laser power levels: 50 mW (~3 mW/mm^2), 100 mW (~5 mW/mm^2), and 300 mW (~15 mW/mm^2). (*C*) Venus expression behavior in embryo and young transgenic medaka before laser irradiation (1) and after laser irradiation (5). Laser power: (2) 50 mW (~3 mW/mm^2), (3) 100 mW (~5 mW/mm^2), (4 and 6) 150 mW (~8 mW/mm^2).

genes used (49). When irradiated with optimized laser power, which raised the temperature to ~42 °C, NIH 3T3 and Colon-26 cells expressed GFP and C6 cells expressed DsRed (Fig. 2*A* and *SI Appendix*, Fig. S4). The optimal temperature of 42 °C for effective gene expression in these cells was determined by their incubation in thermostatic chambers, in which cell viability was not affected at temperatures up to 42 °C (*SI Appendix*, Fig. S5). Transfected NIH 3T3 cells also expressed *Pyrearinus termitilluminans* luciferase (50),

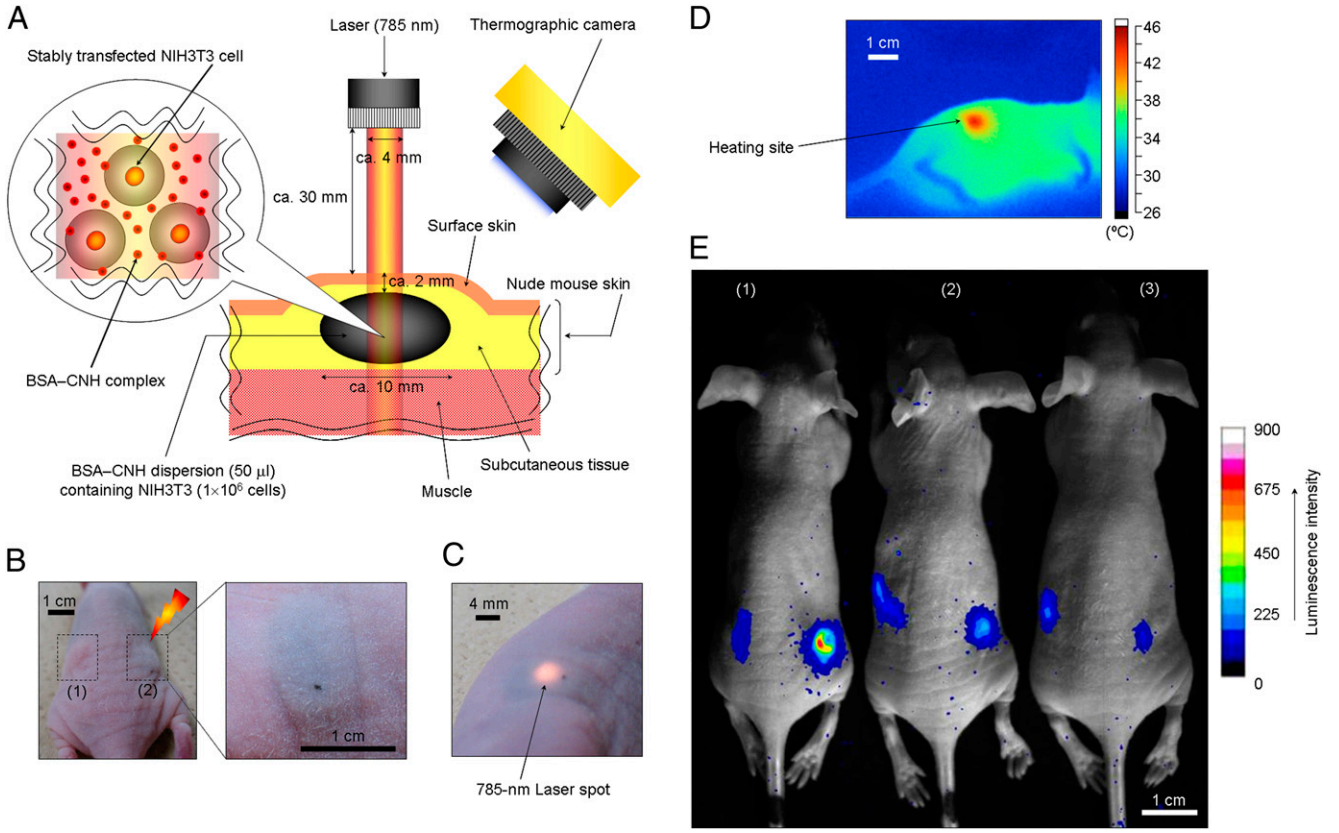

Fig. 3. In vivo gene expression by laser-induced CNH complexes. (*A*) Location and geometry of suspensions consisting of NIH 3T3 cells and CNH complexes inside the tissue. (*B*) Photographs of suspensions consisting of NIH 3T3 cells and CNH complexes injected in a nude mouse. (*C*) Photograph of a 785-nm laser spot on the body of a mouse. (*D*) Thermographic measurement on the mouse's body surface with 785-nm laser-induced CNH complexes [laser power, 150 mW (~12 mW/mm^2); irradiation time, 5 min]. (*E*) Bioimaging of in vivo gene expression driven by photothermal properties of CNH complexes. The right side of the body surfaces of mice were irradiated with a 785-nm laser at three preset temperatures: (1) 42 °C, (2) 39 °C, and (3) 45 °C.

which emits green light (λ_{max}, 538 nm) with D-luciferin as a substrate. Photothermal properties of CNH complexes drive luciferase expression only after application of laser irradiation at 100 mW (5 mW/mm^2) (Fig. 2*B* and *SI Appendix*, Figs. S5*F* and S6). To quantify luciferase expression for each laser power, we monitored luminescence intensity [measured in relative light units (RLU)/min] in real time using a luminometer. In control experiments performed without laser irradiation or BSA–CNH, we observed no significant gene expression. Moreover, the cells irradiated without CNH complexes did not express proteins.

We investigated the laser-induced gene expression behavior of the NIH 3T3 cells encapsulating BSA–CNH complexes to reduce the amount of CNHs administered (*SI Appendix*, Fig. S7). In this system, many CNH complexes were located inside the cells (*SI Appendix*, Fig. S3). Maximum GFP expression was observed at 300 mW (~24 mW/mm^2). We also investigated the photothermic regulation of gene expression by laser-induced BSA–CNH dispersed in 0.3% artificial water in transgenic medaka (Fig. 2*C*). Significant variations in expression of variants of yellow fluorescent protein (Venus) (51) in embryos and young transgenic medaka (52) were observed for each laser power. Maximum Venus expression was observed at 150 mW (~8 mW/mm^2) and ~39 °C. A previous study reported activation of the heat shock promoter at ~39 °C in medaka cells (52). In control experiments without BSA–CNH, the same laser irradiation caused no Venus expression. Thus, these results definitively indicate that gene expression in cells and medaka can be controlled using the photothermal properties of BSA–CNH.

In Vivo Gene Expression by Laser-Induced CNHs. Finally, we investigated in vivo gene expression driven by the photothermal properties of BSA–CNH in a living mouse (Fig. 3). We chose

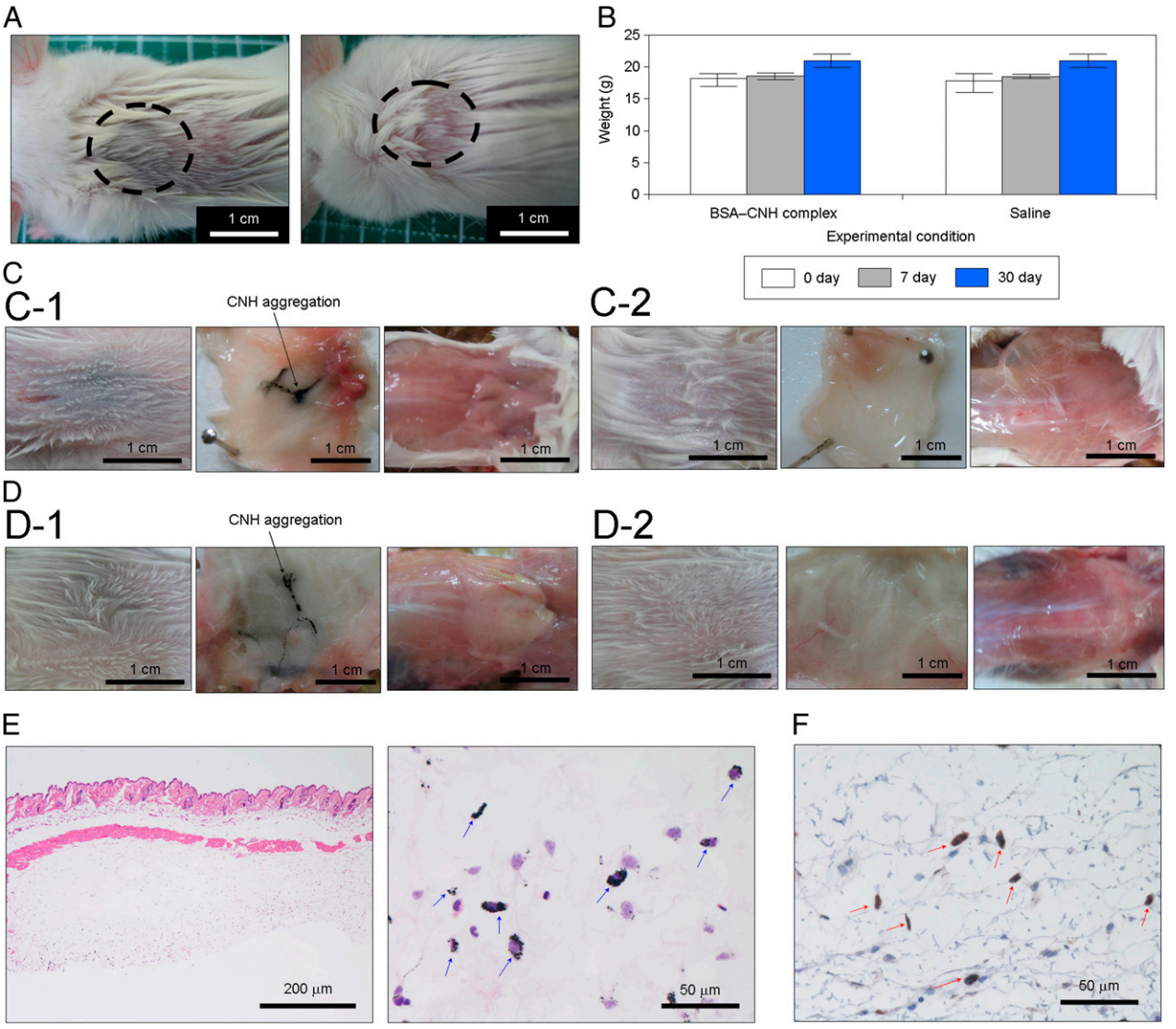

Fig. 4. Biocompatibility of CNH complexes. (*A*) A mouse's back after immediate injection of BSA–CNH complexes (*Left*) and saline (*Right*). (*B*) Weight changes in mice with or without CNH complex injection. (*C*) A mouse's back and anatomic skin tissue at 7 d after BSA–CNH complex dispersion (*C*-1) and saline (*C*-2) injections. (*D*) A mouse's back and anatomic skin tissue at 30 d after BSA–CNH complex dispersion (*D*-1) and saline (*D*-2) injections. (*E* and *F*) Pathological analysis of skin tissue after CNH complex injection. (*E*) Optical microscopy images of skin tissue of mice dissected at 30 d after injection of CNH complexes under the skin. (H&E staining; original magnification: left, 10×; right, 60×.) Blue arrows indicate CNH agglomerates. (*F*) Immunohistochemical detection of macrophages in s.c. tissue of mice dissected at 30 d after injection of CNH complexes under the skin. (Original magnification: 60×.) Red arrows indicate CNH agglomerates with adjacent macrophages.

luciferase as the reporter gene because it provides bioluminescence without background fluorescence and allows highly sensitive detection. Suspensions of BSA–CNH and stably transfected NIH 3T3 cells were injected at two locations on the back of a nude mouse (Fig. 3 *A* and *B*). Almost all of the BSA–CNH complexes were located around the cells, near their surface, because of the slow cellular uptake of the CNH complexes (*SI Appendix*, Fig. S3). Body surface temperature was monitored using a thermographic camera during 785-nm laser irradiation for 30 min [laser output: ~80–200 mW (~6–16 mW/mm^2); preset temperatures: 39, 42, and 45 °C] (Fig. 3 *C* and *D*). After 5 h, NIH 3T3 cells under the skin expressed luciferase, as detected on in vivo bioimaging (Fig. 3*E* and *SI Appendix*, Fig. S8).

To quantify the observed light, we demarcated regions of interest over the cell-injected areas and evaluated the mean luminescence intensity (i.e., total number of photons per pixel in the cell-injected area) in these areas. The maximum luminescence intensity value was obtained at a body surface temperature of 42 °C. The maximum RLU in the cell-injected area under laser irradiation (preset temperature, 42 °C) was approximately sevenfold higher than that in the control experiment without laser irradiation. Meanwhile, the maximum RLU in the cell-injected area was approximately threefold higher at 42 °C than at 39 °C. The luminescence intensity value was lowest at a preset temperature of 45 °C, probably as a result of cell death due to the excess photothermal effects of CNH complexes. Supporting this idea, burn injury appeared near the injected areas only at 45 °C (*SI Appendix*, Fig. S9). BSA–CNH is nontoxic, as demonstrated by various biocompatibility analyses, including blood investigations, weight determinations, and pathological examinations (Fig. 4 and Table 1). Careful visual observations revealed no signs of inflammatory reaction against BSA–CNH, but did identify a large CNH aggregation encapsulated by s.c. tissue (Fig. 4*A*). Virtually no changes in the weight of mice with and without injections of CNH complexes were seen (Fig. 4*B*), and no histological abnormalities, such as granulomas or fibrosis, were observed (Fig. 4 *C* and *D*). H&E staining confirmed a wide distribution of CNH throughout the s.c. tissue (Fig. 4*E*). Immunohistochemical staining revealed the absence of undesired inflammatory responses, although CNH uptake by macrophages (41, 42) stained with rabbit anti-ionized calcium binding adaptor molecule 1 was observed (53) (Fig. 4*F*). Furthermore, complete blood cell count and biochemical examinations of BSA–CNH were all normal, at least for 30 d (Table 1). In particular, virtually no changes in levels of inflammatory markers (i.e., WBC and C-reactive protein) were seen after injection of BSA–CNH.

These results clearly demonstrate that CNH complexes have low toxicity, at least for 30 d. However, we recently reported that CNHs are highly accumulated in the organs of the reticuloendothelial system (43). In addition, Lacotte et al. (41) reported activation of immunocompetent cells by chemically functionalized CNHs. Thus, further detailed studies on the biocompatibility of CNHs (e.g., high doses and long-term use) are needed to obtain a conclusive answer. In any case, we have demonstrated that BSA–CNH effectively causes a temperature increase in mice by channeling the powerful photothermal effect of CNH, thereby stimulating significant in vivo gene expression.

Conclusions

In the present study, we have successfully developed a unique gene expression system that uses the photothermal properties of water-dispersible BSA–CNH complexes and operates through a heat shock promoter. The complexes enable remote in vitro gene expression in various cells and transgenic medaka by external laser irradiation. Moreover, we successfully controlled gene expression remotely in a mice using a low-power laser that can penetrate living tissue. We believe that this is a unique demonstration of remote control of gene expression that relies on the powerful photothermal properties of nanomaterials. This work is a proof-of-principle study demonstrating that in vitro and in vivo gene expression can be mediated by the photothermal properties of nanocarbons. Further studies are needed to investigate efficient laser irradiation systems and appropriate stereotactic administration of cells and nanocarbons within an organism to determine the effective expression of various target genes in a deep tissue for advanced optogenetics and therapeutics. Future technological advances might allow temporospatial in vivo expression and regulation of various genes inserted downstream of heat shock promoters. On the other hand, it is well known that HSPs are the most attractive biomolecules as therapeutic targets and therapeutic agents (14–18). Herein, heat shock promoter-mediated gene expression system is going to be a powerful activator in health and diseases. This study has identified a potent tool for application in various biological fields, including analysis of cell signaling within organisms, investigation of genetic mechanisms, and development of unique cell therapies and tissue engineering techniques.

Methods

Detailed information on functional nanocarbon complexes, characterization of BSA–CNH, temperature assays, plasmid construction, cell cultures and stable transfections, cellular uptake of CNH complexes, cytotoxicity tests of nanocarbon complexes, in vitro laser experiments, and animal experiments is provided in *SI Appendix*.

Table 1. CBC and biochemical examination of mice after injections of BSA–CNH complexes or saline

			BSA–CNH complex		Saline	
Method	Entry	Unit	After 7 d	After 30 d	After 7 d	After 30 d
CBC	WBC	Cells/μL	3,000	3,167	3,433	2,750
Biochemical examination	CRP	mg/L	0.1	0.4	0.2	0.1
	AST	IU/L	53	52	68	47
	ALT	IU/L	22	32	30	35
	LDH	IU/L	539	492	592	539
	Amylase	IU/L	1,775	2,347	1,923	1,865
	CK	IU/L	217	155	160	162
	Total protein	mg/L	54	49	54	48
	Albumin	mg/L	45	36	45	36
	BUN	mg/L	192	204	173	205
	Creatinine	mg/L	0.9	1	0.9	1.1

Data are average values from five experiments. ALT, alanine aminotransferase; AST, aspartate aminotransferase; BUN, Blood urea nitrogen; CK, creatine kinase; CRP, C-reactive protein; LDH, lactate dehydrogenase.

ACKNOWLEDGMENTS. We thank Dr. Hirobumi Suzuki (Olympus) for providing the pHsp70-luc2, Keiko Nishio and Mari Sasao (Health Research Institute, National Institute of Advanced Industrial Science and Technology) for assisting with the experiments, and NEC for providing the carbon nanohorn. This work was supported by the Japan Prize Foundation and Grant-in-Aid for Young Scientists B 23700568.

1. Stringham EG, Candido EP (1993) Targeted single-cell induction of gene products in *Caenorhabditis elegans*: A new tool for developmental studies. *J Exp Zool* 266: 227–233.
2. Harris J, Honigberg L, Robinson N, Kenyon C (1996) Neuronal cell migration in *C. elegans*: Regulation of Hox gene expression and cell position. *Development* 122:3117–3131.
3. Halfon MS, Kose H, Chiba A, Keshishian H (1997) Targeted gene expression without a tissue-specific promoter: Creating mosaic embryos using laser-induced single-cell heat shock. *Proc Natl Acad Sci USA* 94:6255–6260.
4. Halloran MC, et al. (2000) Laser-induced gene expression in specific cells of transgenic zebrafish. *Development* 127:1953–1960.
5. Leitz G, Fällman E, Tuck S, Axner O (2002) Stress response in *Caenorhabditis elegans* caused by optical tweezers: Wavelength, power, and time dependence. *Biophys J* 82: 2224–2231.
6. Ramos DM, Kamal F, Wimmer EA, Cartwright AN, Monteiro A (2006) Temporal and spatial control of transgene expression using laser induction of the *hsp70* promoter. *BMC Dev Biol* 6:55.
7. Kamei Y, et al. (2009) Infrared laser-mediated gene induction in targeted single cells *in vivo*. *Nat Methods* 6:79–81.
8. Deguchi T, et al. (2009) Infrared laser-mediated local gene induction in medaka, zebrafish and *Arabidopsis thaliana*. *Dev Growth Differ* 51:769–775.
9. Ebbinghaus S, Dhar A, McDonald JD, Gruebele M (2010) Protein folding stability and dynamics imaged in a living cell. *Nat Methods* 7:319–323.
10. Bruegmann T, et al. (2010) Optogenetic control of heart muscle *in vitro* and *in vivo*. *Nat Methods* 7:897–900.
11. Boyden ES, Zhang F, Bamberg E, Nagel G, Deisseroth K (2005) Millisecond-timescale, genetically targeted optical control of neural activity. *Nat Neurosci* 8:1263–1268.
12. Ye H, Daoud-El Baba M, Peng RW, Fussenegger MA (2011) A synthetic optogenetic transcription device enhances blood-glucose homeostasis in mice. *Science* 332: 1565–1568.
13. Huang H, Delikanli S, Zeng H, Ferkey DM, Pralle A (2010) Remote control of ion channels and neurons through magnetic-field heating of nanoparticles. *Nat Nanotechnol* 5:602–606.
14. Morimoto RI, Santoro MG (1998) Stress-inducible responses and heat shock proteins: New pharmacologic targets for cytoprotection. *Nat Biotechnol* 16:833–838.
15. Rylander MN, Stafford RJ, Hazle J, Whitney J, Diller KR (2011) Heat shock protein expression and temperature distribution in prostate tumours treated with laser irradiation and nanoshells. *Int J Hyperthermia* 27:791–801.
16. Rylander MN, Feng Y, Zimmermann K, Diller KR (2010) Measurement and mathematical modeling of thermally induced injury and heat shock protein expression kinetics in normal and cancerous prostate cells. *Int J Hyperthermia* 26:748–764.
17. Sõti C, et al. (2005) Heat shock proteins as emerging therapeutic targets. *Br J Pharmacol* 146:769–780.
18. Pockley AG (2001) Heat shock proteins in health and disease: Therapeutic targets or therapeutic agents? *Expert Rev Mol Med* 3:1–21.
19. König K (2000) Multiphoton microscopy in life sciences. *J Microsc* 200:83–104.
20. Weissleder R (2001) A clearer vision for *in vivo* imaging. *Nat Biotechnol* 19:316–317.
21. Kam NWS, O'Connell M, Wisdom JA, Dai H (2005) Carbon nanotubes as multifunctional biological transporters and near-infrared agents for selective cancer cell destruction. *Proc Natl Acad Sci USA* 102:11600–11605.
22. Burke A, et al. (2009) Long-term survival following a single treatment of kidney tumors with multiwalled carbon nanotubes and near-infrared radiation. *Proc Natl Acad Sci USA* 106:12897–12902.
23. Sarkar S, et al. (2011) Measurement of the thermal conductivity of carbon nanotube–tissue phantom composites with the hot wire probe method. *Ann Biomed Eng* 39: 1745–1758.
24. Sarkar S, Gurjarpadhye AA, Rylander CG, Nichole Rylander M (2011) Optical properties of breast tumor phantoms containing carbon nanotubes and nanohorns. *J Biomed Opt* 16:051304.
25. Whitney JR, et al. (2011) Single-walled carbon nanohorns as photothermal cancer agents. *Lasers Surg Med* 43:43–51.
26. Zhang M, et al. (2008) Fabrication of ZnPc/protein nanohorns for double photodynamic and hyperthermic cancer phototherapy. *Proc Natl Acad Sci USA* 105: 14773–14778.
27. Miyako E, et al. (2007) Near-infrared laser-triggered carbon nanohorns for selective elimination of microbes. *Nanotechnology* 18:475103.
28. Miyako E, et al. (2008) Photoinduced antiviral carbon nanohorns. *Nanotechnology* 19: 075106.
29. Miyako E, et al. (2011) A photo-thermal-electrical convertor based on carbon nanotubes for bioelectronic applications. *Angew Chem Int Ed* 51:2266–12270.
30. Miyako E, Nagata H, Hirano K, Hirotsu T (2008) Carbon nanotube–polymer composite for light-driven microthermal control. *Angew Chem Int Ed Engl* 47:3610–3613.
31. Miyako E, Nagata H, Hirano K, Hirotsu T (2009) Micropatterned carbon nanotube–gel composite as photothermal material. *Adv Mater (Deerfield Beach Fla)* 21:2819–2823.
32. Miyako E, Nagata H, Hirano K, Hirotsu T (2009) Laser-triggered carbon nanotube microdevice for remote control of biocatalytic reactions. *Lab Chip* 9:788–794.
33. Miyako E, Nagata H, Hirano K, Hirotsu T (2008) Photodynamic thermoresponsive nanocarbon–polymer gel hybrids. *Small* 4:1711–1715.
34. Miyako E, Nagata H, Funahashi R, Hirano K, Hirotsu T (2009) Carbon nanotube–polymer gel hybrid–based light-triggered thermoelectric conversion. *ChemSusChem* 2:419–422.
35. Miyako E, Nagata H, Funahashi R, Hirano K, Hirotsu T (2009) Light-driven thermoelectric conversion based on a carbon nanotube–ionic liquid gel composite. *ChemSusChem* 2:740–742.
36. Miyako E, Itoh T, Nara Y, Hirotsu T (2009) Ionic liquids on photoinduced nanotube composite arrays as a reaction medium. *Chemistry* 15:7520–7525.
37. Miyako E, Nagata H, Hirano K, Makita Y, Hirotsu T (2008) Photodynamic release of fullerenes from within carbon nanohorn. *Chem Phys Lett* 456:220–222.
38. Robinson JT, et al. (2010) High performance *in vivo* near-IR (>1 μm) imaging and photothermal cancer therapy with carbon nanotubes. *Nano Res* 3:779–793.
39. Colvin VL (2003) The potential environmental impact of engineered nanomaterials. *Nat Biotechnol* 21:1166–1170.
40. Poland CA, et al. (2008) Carbon nanotubes introduced into the abdominal cavity of mice show asbestos-like pathogenicity in a pilot study. *Nat Nanotechnol* 3:423–428.
41. Lacotte S, et al. (2008) Interfacing functionalized carbon nanohorns with primary phagocytic cells. *Adv Mater (Deerfield Beach Fla)* 20:2421–2426.
42. Tahara Y, et al. (2011) Histological assessments for toxicity and functionalization-dependent biodistribution of carbon nanohorns. *Nanotechnology* 22:265106.
43. Miyawaki J, Yudasaka M, Azami T, Kubo Y, Iijima S (2008) Toxicity of single-walled carbon nanohorns. *ACS Nano* 2:213–226.
44. Isobe H, et al. (2006) Preparation, purification, characterization, and cytotoxicity assessment of water-soluble, transition-metal–free carbon nanotube aggregates. *Angew Chem Int Ed Engl* 45:6676–6680.
45. Zhang M, Yudasaka M, Ajima K, Miyawaki J, Iijima S (2007) Light-assisted oxidation of single-wall carbon nanohorns for abundant creation of oxygenated groups that enable chemical modifications with proteins to enhance biocompatibility. *ACS Nano* 1: 265–272.
46. Murphy FA, et al. (2011) Length-dependent retention of carbon nanotubes in the pleural space of mice initiates sustained inflammation and progressive fibrosis on the parietal pleura. *Am J Pathol* 178:2587–2600.
47. Nagai H, et al. (2011) Diameter and rigidity of multiwalled carbon nanotubes are critical factors in mesothelial injury and carcinogenesis. *Proc Natl Acad Sci USA* 108: E1330–E1338.
48. Shimomura O, Johnson FH, Saiga Y (1962) Extraction, purification and properties of aequorin, a bioluminescent protein from the luminous hydromedusan, *Aequorea*. *J Cell Comp Physiol* 59:223–239.
49. Matz MV, et al. (1999) Fluorescent proteins from nonbioluminescent *Anthozoa* species. *Nat Biotechnol* 17:969–973.
50. Nakajima Y, et al. (2010) Enhanced beetle luciferase for high-resolution bioluminescence imaging. *PLoS ONE* 5:e10011.
51. Nagai T, et al. (2002) A variant of yellow fluorescent protein with fast and efficient maturation for cell-biological applications. *Nat Biotechnol* 20:87–90.
52. Oda S, et al. (2010) Identification of a functional medaka heat shock promoter and characterization of its ability to induce exogenous gene expression in medaka *in vitro* and *in vivo*. *Zoolog Sci* 27:410–415.
53. Kanazawa H, Ohsawa K, Sasaki Y, Kohsaka S, Imai Y (2002) Macrophage/microglia-specific protein Iba1 enhances membrane ruffling and Rac activation via phospholipase C-γ–dependent pathway. *J Biol Chem* 277:20026–20032.